ARTICLE

Check for updates

The climate sensitivity of northern Greenland fjords is amplified through sea-ice damming

Christian Stranne [1,2 ✉], Johan Nilsson[2,3], Adam Ulfsbo [4], Matt O'Regan [1,2], Helen K. Coxall [1,2], Lorenz Meire [5,6], Julia Muchowski [1,2], Larry A. Mayer[7], Volker Brüchert [1,2], Jonas Fredriksson [1,2], Brett Thornton [1,2], Julek Chawarski [8], Gabriel West [1,2], Elizabeth Weidner[1,2,7] & Martin Jakobsson [1,2]

Record-high air temperatures were observed over Greenland in the summer of 2019 and melting of the northern Greenland Ice Sheet was particularly extensive. Here we show, through direct measurements, that near surface ocean temperatures in Sherard Osborn Fjord, northern Greenland, reached 4 °C in August 2019, while in the neighboring Petermann Fjord, they never exceeded 0 °C. We show that this disparity in temperature between the two fjords occurred because thick multi-year sea ice at the entrance of Sherard Osborn Fjord trapped the surface waters inside the fjord, which led to the formation of a warm and fresh surface layer. These results suggest that the presence of multi-year sea ice increases the sensitivity of Greenland fjords abutting the Arctic Ocean to climate warming, with potential consequences for the long-term stability of the northern sector of the Greenland Ice Sheet.

[1] Department of Geological Sciences, Stockholm University, Stockholm, Sweden. [2] Bolin Centre for Climate Research, Stockholm, Sweden. [3] Department of Meteorology, Stockholm University, Stockholm, Sweden. [4] Department of Marine Sciences, University of Gothenburg, Gothenburg, Sweden. [5] Greenland Climate Research Centre, Greenland Institute of Natural Resources, Nuuk, Greenland. [6] Department of Estuarine and Delta Systems, NIOZ Royal Netherlands Institute of Sea Research, Yerseke, The Netherlands. [7] Center for Coastal and Ocean Mapping, University of New Hampshire, Durham, NH, USA. [8] Fisheries and Marine Institute of Memorial University of Newfoundland, St. John's, Canada. ✉email: christian.stranne@geo.su.se

The Lincoln Sea is a continental shelf sea of the Arctic Ocean, fringing northern Greenland, and abutted by several large outlet glaciers that drain the North Greenland ice sheet. The region is renowned for its persistent and thick sea ice cover (Fig. 1). Although Arctic Ocean sea ice extent and volume has been in rapid decline over the past few decades[1–3], ice conditions in the Lincoln Sea have remained heavy due to the large-scale sea ice transport patterns, dominated by the Beaufort Gyre (BG) and the Transpolar Drift (TPD), that transport sea-ice towards northern Greenland (Fig. 1). The Lincoln Sea is predicted to be the last outpost for multi-year sea ice (MYI) in the Arctic, which has decreased by more than 50% in coverage since 1999 across the Arctic Ocean[1,4–6]. Despite the relative stability of sea-ice in the Lincoln Sea, accelerated ice-mass loss from outlet glaciers of the North Greenland Ice Sheet has occurred over the past 10–15 years[7]. This area is therefore of great interest for monitoring both sea ice and glacier conditions and cascading changes to regional physical and biogeochemical processes that might have unexpected implications for the wider Arctic cryosphere and ecosystems.

While changes in sea ice, glacier, and atmospheric conditions can be monitored remotely using satellites, direct and detailed oceanographic, chemical and biological observations are essential to address the driving mechanisms and consequences of rising air temperatures. With modal sea ice thicknesses (i.e., the dominant ice thickness) often reaching well above 4 m[4], the Lincoln Sea region remains, however, one of the least explored parts of the world's oceans. Only 21 hydrographic stations exist within the Lincoln Sea in the World Ocean Database 2018[8] (WOD18), excluding stations that only cover observational depths >50 m. Here we present data from 97 hydrographic stations distributed over Nares Strait (30), Lincoln Sea (3), Petermann Fjord (39), and Sherard Osborn Fjord (SOF, 25) along with continuous

measurements of near sea-surface temperatures (NST) obtained from the Swedish icebreaker (IB) *Oden* during expeditions in 2015 and 2019 (Fig. 1). During the *Ryder 2019 Expedition*, IB *Oden* became the first ship to enter SOF to collect a broad range of scientific data[9]. We present hydrographic and biogeochemical data collected in SOF and place them into a larger, regional, context. Satellite data and reanalysis products indicate that the summer of 2019 in the SOF area was extreme in terms of near-surface air temperature (T_{2m}) and sea ice concentration (*SIC*). Our in situ measurements complement these observations to provide a detailed picture of local processes and the impacts of rapid climate warming in this region.

Results and discussion

Ryder Glacier drains into SOF, which is ~17 km wide and ~55 km long, measured from the glacier's ice tongue margin in 2019 to the fjord mouth in line with Castle Island (Fig. 1 and Supplementary Fig. S1). The fjord has a glacially excavated inner basin, with a maximum depth of 890 m, and a sill restricting the connection to the Lincoln Sea. The deepest water passage across this sill is 475 m deep and located on the western side of two small islands at the center of the fjord mouth[10].

Mean July–August T_{2m} extracted from the ERA5 reanalysis[11] over the study area reveal a clear warming trend between 1979–2019, with a 0.7 °C increase per decade (Fig. 2a). This trend is 2.5x steeper (and significantly different with a *p*-value of 0.016) from the trend in the global average land-surface air temperature (CRUTEM4[12]) over the same period (Supplementary Fig. S2). The steeper trend is related to a phenomenon known as Arctic amplification[13–16] and is within the expected range, around 2x the global trend based on observations[17–19] and 3–4x the global trend over a longer time perspective using paleo-reconstructions[20]. In 2019, the mean summer T_{2m} in the SOF area
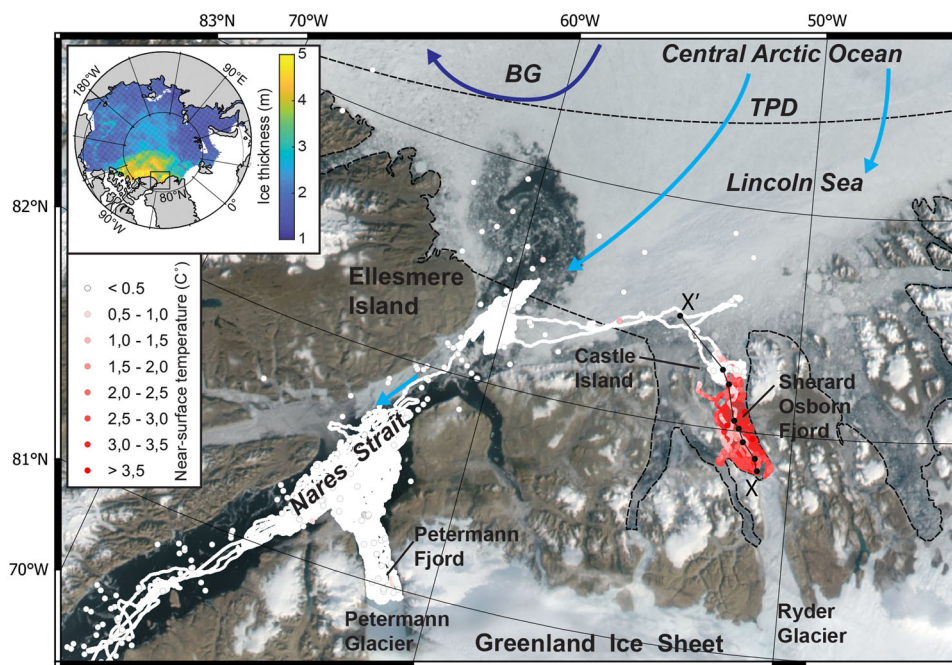

Fig. 1 Map of Nares Strait and the Lincoln Sea. The cruise tracks from the two recent expeditions with Icebreaker Oden 2015 and 2019 are shown with colors based on measured under-hull temperature (see methods section). Filled circles represent the maximum near-surface (<20 m) temperature from discrete hydrographic stations taken during these expeditions, as well as from World Ocean Database 2018[8]. The background is a MODIS-Terra corrected reflectance (true color) image. The inset shows sea ice thickness in the Arctic Ocean, averaged over one month, 15 September to 15 October 2019 (based on CryoSat-2 data[42]). Arrows show large-scale sea ice drift patterns with Beaufort Gyre (BG) and Transpolar Drift (TPD), and a dashed black line marks the Lincoln Sea border. We acknowledge the use of imagery from the NASA Worldview application (https://worldview.earthdata.nasa.gov), part of the NASA Earth Observing System Data and Information System (EOSDIS).
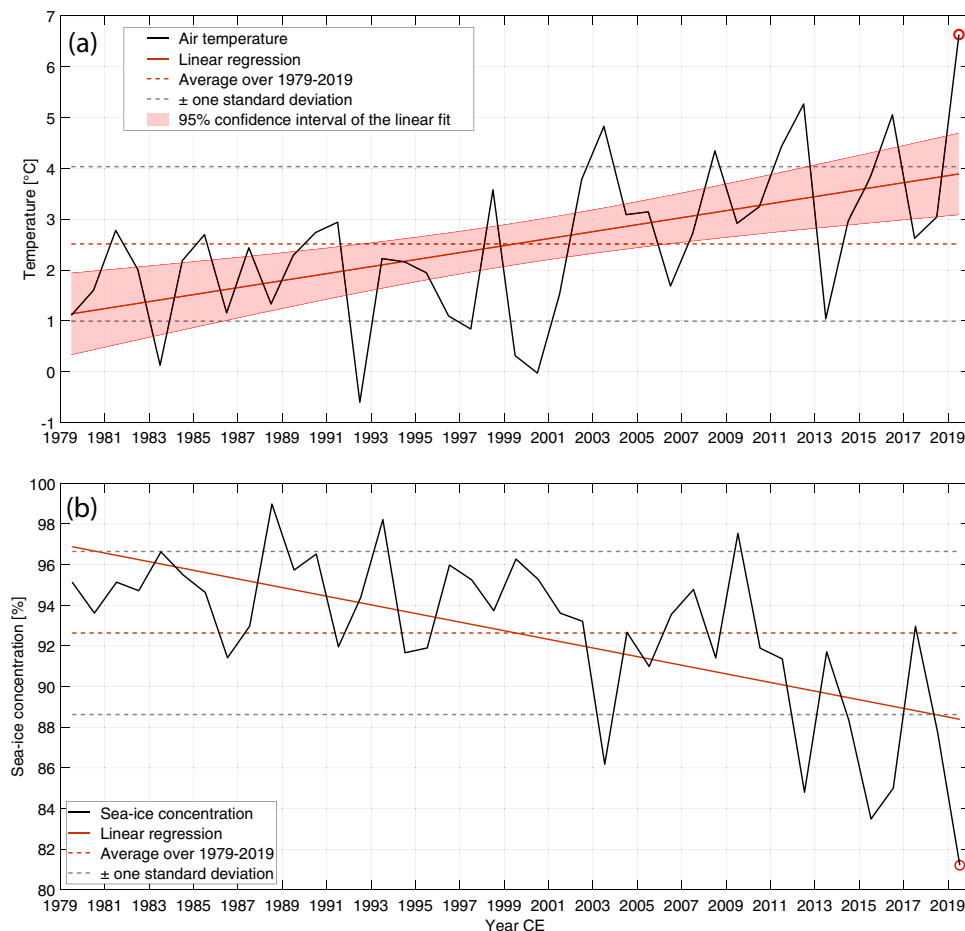
Fig. 2 Time series of atmospheric conditions. a Mean June–August T_{2m} from the ERA5 reanalysis averaged over the Sherard Osborn Fjord area, outlined in Fig. 4f. **b** Mean July–August sea ice concentration from Copernicus Climate Change Service, derived from satellite sensor data, and averaged over three grid points are shown in Fig. 4f.

reached 6.6 °C, the highest in the time series and more than 4 °C (and 2.7 standard deviations) above the 1979–2019 average. A similar, but negative, trend can be seen for the average July–August *SIC* in SOF derived from satellite sensor data[11] (Fig. 2b). The summer of 2019 shows the lowest *SIC* on the 1979–2019 record, almost three standard deviations below the average (Fig. 2b). Tedesco and Fettweis[21] showed that these high air temperatures and low sea ice concentrations in northern Greenland were caused by the persistence of a high-pressure system during the summer, which favored the advection of warm and wet air along the Greenland west coast towards the north. Consequently, the Greenland Ice Sheet mass loss in 2019 was the highest on record[22].

How did the extreme *SIC* and T_{2m} conditions of 2019 influence the marine physical and biogeochemical state of the SOF? Firstly, the near-surface ocean temperatures (NST) we measured in SOF appear to have been anomalously high (Figs. 1, 3a, 4c). Here we define NST as the maximum temperature in the top 20 m of the water column, which catches a warm near-surface signal, even if there is a cold freshwater layer on top. NST's in the 2019 CTD (Conductivity, Temperature, Depth) data from inside SOF (25 stations) reached above 3.8 °C (Fig. 4c). Within the area bounded by 81 and 83 °N and by 45 and 65 °W, covering roughly northern Nares Strait, the Lincoln Sea, Petermann Fjord, and SOF (dashed red boundary in Fig. 4f) we found a total of 373 ocean temperature profiles in WOD18, collected between 1948 and 2019. Including five stations not included in WOD18 (from a research project named Switchyard), the average NST in these profiles is −1.3 ± 0.5 °C and the maximum NST in these historical

records is 1.0 °C. In a regional context, the observations made in SOF in 2019 are exceptionally warm, with temperatures reaching about 3 °C higher than previously recorded in any ocean waters off northern Greenland. It is worth noting that this is a comparison between the more isolated SOF and an area that includes more open ocean conditions in northern Nares Strait and the Lincoln Sea. In the neighboring Petermann Fjord the average NST (53 profiles collected between 1970 and 2019, including those collected during the *Petermann 2015* and *Ryder 2019* expeditions) is indeed slightly higher than the regional average, −0.5 ± 0.6 °C with a maximum of 0.9 °C, but substantially lower than those we observed in SOF.

Why are NSTs in SOF (red interval, Fig. 4c) so much higher than just outside the fjord, in the Lincoln Sea (green interval, Fig. 4c)? One obvious difference between the two areas is the significantly lower sea ice concentration in SOF during the summer of 2019, which is in stark contrast to the heavy MYI conditions in the Lincoln Sea (Fig. 1). Without sea ice cover in the fjord, the ocean absorbs more incoming solar radiation, due to the lower surface albedo, resulting in locally elevated temperatures and further sea ice melt, a mechanism known as surface albedo feedback. The integrated heat content over the top ~15 m of the water column, with reference to the freezing temperature and normalized over the integration depth for each CTD profile, is shown in Fig. 4a (see Supplementary Note for details). The heat content provides a more robust measure of the temperature conditions in the surface layer, but these data are only available at the discrete CTD stations while NST, estimated from the hull
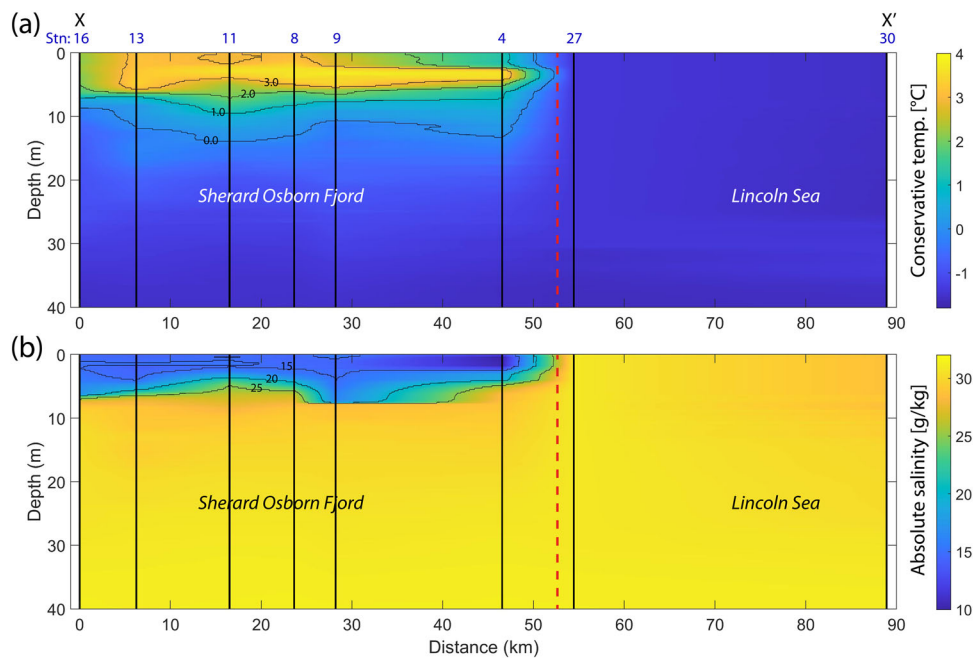
Fig. 3 Hydrographic data from Sherard Osborn Fjord. Transect along Sherard Osborn Fjord from X to X' (shown in Fig. 1) based on CTD data of (**a**) conservative temperature and (**b**) absolute salinity. Black vertical lines indicate individual CTD profiles (with corresponding station number in blue) and the dashed red line corresponds to the front position shown in Fig. 4g.
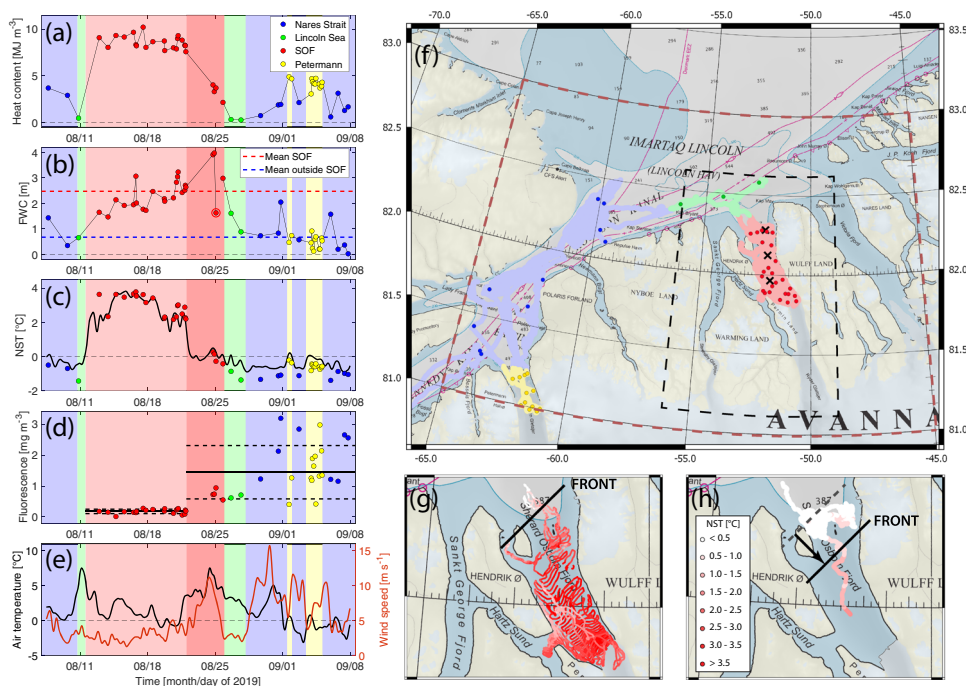

Fig. 4 Near-surface ocean and atmospheric data. Upper-ocean (**a**) heat content and (**b**) freshwater content (FWC), based on CTD data. **c** Near-surface temperature (NST) from CTD data (colored circles) and estimated from hull temperature (black line). **d** Average fluorescence from CTD (integrated and normalized in the same way as heat content). Also shown are the average (solid black) and ±one standard deviation (dashed black) for the first part of Sherard Osborn Fjord (SOF) and for the rest. Note that we do not have data from the first three CTD stations. **e** Shipboard observations of air temperature (black) and wind speed (red). The colored intervals in **a**–**e** correspond to areas surveyed during the Ryder 2019 expedition shown in **f**. Note that the northwestern part of the cruise track is blue although it is formally inside the Lincoln Sea (cf. Fig. 1). Also shown in **f** is the SOF area over which summer T_{2m} is calculated (dashed black), the area over which the average historic NST is calculated (dashed red), and the three grid points used for calculating SIC (black crosses). **g** Hull temperatures during the first part within SOF (light red interval in **a**–**e**) and (**h**) hull temperatures during the last part within SOF (dark red interval in **a**–**e**). Shipboard observations in **c** and **e** were collected at 1/60 Hz and were low-pass filtered with a binomial filter to reduce diurnal variability and other higher frequency fluctuations. The CTD profile at the data point with the red circle in **b** (around August 25) begins at a depth of 5.6 m and did not catch the very fresh surface layer seen in the surrounding profiles, hence the comparably low FWC.

temperature (at about 6 m below the sea surface), is available continuously along the cruise track (Fig. 4c). The hull temperature is a decent proxy for NST, although it tends to overestimate low temperatures and underestimate high temperatures (Fig. 4c). The heat content in the Lincoln Sea was close to zero J m^{-2}, meaning that the water in the surface layer was close to the freezing point. In SOF, the heat content was higher, especially during the first part of our measuring campaign within the fjord (light red interval in Fig. 4a). The sharp drop in NST, seen at the beginning of the dark red interval in Fig. 4c, occurred when *IB Oden* moved from inner to outer SOF. The temperature decrease in surface water in outer SOF was presumably primarily associated with a frontal shift that brought cool Lincoln Sea surface waters further into the fjord, rather than by local cooling processes (Fig. 4f–g). This interpretation is supported by the fact that near-surface fluorescence in the outer SOF shows a resemblance to Lincoln Seawater in the later measurements (Fig. 4d).

The surface layer freshwater content in SOF is significantly larger than outside the fjord, as shown by the freshwater height (Fig. 4b, see Supplementary Note for details), with more than twice as much freshwater inside SOF (compare dashed blue and red lines in Fig. 4b). The surface freshwater pool inside SOF (Figs. 3b, 5a) is likely created by local freshwater input from terrestrial runoff and local sea ice and iceberg melt. However, such a buoyant freshwater layer would tend to spread laterally and flow out of the fjord, and therefore a continuous freshwater input is needed to sustain the pool. By using a conceptual two-layer model[23,24] we analyze the timescale of the surface freshwater layer and the freshwater input needed to maintain it in steady-state (Supplementary Note). The model suggests that it takes about two weeks to build up the surface freshwater pool and that a freshwater input on the order of

5000–10,000 m^3 s^{-1} is needed to maintain a steady-state freshwater height in the observed range of 2–3 m. Based on published results and an iceberg-melt model, we estimate that the summer freshwater input to the surface layer in SOF, sourced from terrestrial runoff, iceberg, sea ice, and ice tongue melt, lies in the range 300–700 m^3 s^{-1}; see the Supplementary Note and Supplementary Fig. S3. We, therefore, deem it unlikely that the freshwater input to SOF in the summer of 2019 actually reached 5000 to 10,000 m^3 s^{-1} as suggested by the conceptual model.

A possible explanation for the excess freshwater in SOF is that the thick MYI outside the fjord (Fig. 1 and Supplementary Fig. S1) acted to trap the warm and fresh surface layer. If the thickness of the fresh surface layer is H and the draft of the sea-ice is h, then the outflow from the surface layer should be reduced by the factor $b = (1 - h/H)^2$. The required freshwater input to maintain a steady-state is substantially reduced by the damming effect of the sea-ice outside the fjord (see Supplementary Note for details): for a sea ice draft of 4 m, the conceptual model yields a steady-state freshwater height of around 2.5 m for freshwater inputs in the range 100–300 m^3 s^{-1} (see Supplementary Figs. S4–7). The model suggests that with a sea ice draft of between 2 and 4 m, a freshwater height in the observed range of 2–3 m can be maintained by an estimated freshwater input to SOF of 300–700 m^3 s^{-1}. Generally, the sea-ice damming causes a fresher surface layer, with a stronger vertical salinity gradient, which acts to reinforce the surface warming by reducing the mixing with colder water from below. Several kilometer-sized icebergs that had broken off the ice tongue drifted around in SOF, as well as smaller icebergs that were trapped by the sea-ice near the fjord mouth, may have contributed to damming the warm, fresh surface pool inside the fjord.
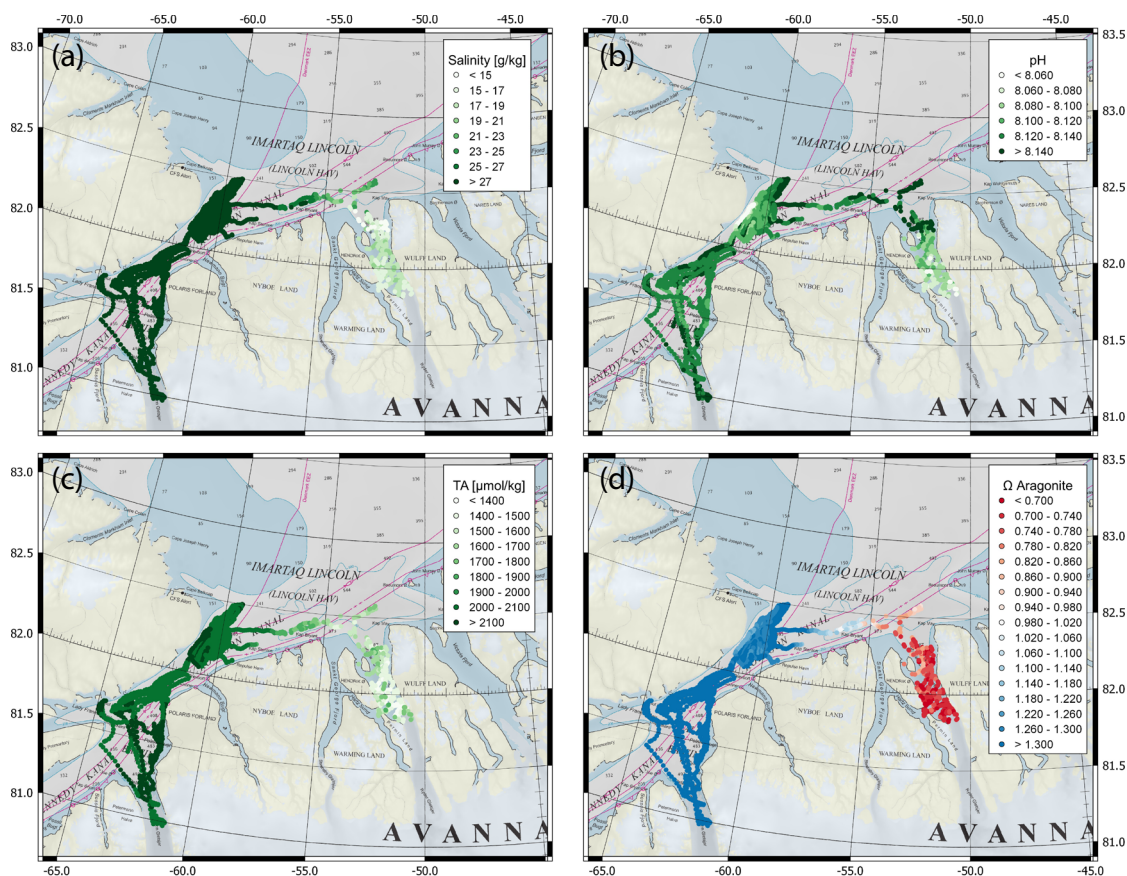

Fig. 5 Near-surface ocean chemistry data. Underway measurements of (**a**) absolute salinity (g/kg), (**b**) seawater pH, (**c**) TA (µmol/kg), and (**d**) Ω_{Ar}. Data are the same as the colored lines in Supplementary Fig. S8 (see the caption for more information on data processing).

These analyses suggest that sea-ice and iceberg damming of the outflow in the surface layer can be a crucial factor for explaining the anomalously low surface salinities and high NST's observed in SOF (Fig. 3). In Petermann Fjord, the freshwater content was not higher than outside the fjord in Nares Strait (Fig. 4b) and NST's were below zero (Fig. 4c). As there was no sea ice outside Petermann Fjord, this supports the idea that the MYI outside SOF is responsible for the warm freshwater pool. Furthermore, Moon et al.[25] showed that the freshwater flux to the Helheim–Sermilik glacier–fjord system in southeast Greenland, including subglacial discharge and iceberg melt was >1500 $m^3 s^{-1}$ in August 2010. Despite this large freshwater input, there is no sign of a warm surface pool inside the Helheim–Sermilik fjord system (surface temperature does not exceed 1.5 °C). The area outside this fjord is not dominated by perennial MYI, which gives further support to the hypothesis that sea-ice damming is responsible for the anomalously warm and fresh surface water observed inside SOF.

The sea-ice damming mechanism bears resemblance to epishelf lakes[26] that are found primarily in ice-free areas between land and floating ice shelves where a thick freshwater layer develops over seawater. In this respect, the warm freshwater pool observed in SOF can be termed a "proglacial lake". Anomalously high NSTs have also been reported in a fjord in northeast Greenland[27] and it seems plausible that those observations may also have been related to sea-ice damming, as MYI was also reported outside that fjord system. It should be noted, however, that the proposed blocking effect can be reduced in a warming climate if the MYI coverage in the Lincoln Sea is reduced.

Ocean chemistry and potential ecological consequences. The anomalous NST's and low near-surface salinity in SOF are particularly reflected in low total alkalinity (TA) and dissolved inorganic carbon (DIC) surface values and generally associated with lower surface pH values (Fig. 5 and Supplementary Fig. S8). As a result, the saturation state of the calcium carbonate polymorph aragonite (Ω_{Ar}), calculated from pH and TA, is well below saturation in the near-surface (Fig. 5d). The near-surface calcium carbonate-corrosive water of SOF has low pH buffering capacity (illustrated by the explicit buffer factors, Supplementary Fig. S9), implying that near-surface Ω_{Ar} inside SOF is twice as sensitive to ocean acidification from the uptake of atmospheric carbon dioxide (CO_2) compared to the region outside the fjord (see Supplementary Note). Freshwater from melted sea-ice and glacial meltwater is usually characterized by both lower TA and DIC concentrations compared to Arctic rivers[28]. The low salinity lens observed in SOF explains the low saturation state of Ω_{Ar} as also observed in other systems impacted by sea-ice and glacial ice melt[29,30]. Such an undersaturation of surface waters imposes constraints on organisms that secrete aragonite to build their skeletal material, such as pteropods[31–33], which are important in Arctic Ocean food webs[34], including within fjords[32]. The warm freshwater pool in SOF would therefore limit the success of calcifying organisms and thereby affect the planktonic food webs inside the fjord. Consistently low fluorescence within SOF (Fig. 4d Supplementary Fig. S10c) may be an indication of impacts on primary production, but further analyses are needed in order to draw conclusions regarding the ecological state of SOF during our measuring campaign.

Effects of sea ice free summers in SOF on ice tongue calving and glacier stability. The high sensitivity of local NST's to atmospheric forcing in SOF is related to the absence of summer sea ice inside the fjord and trapping of warm and fresh surface water by sea ice outside the fjord. These mechanisms, which amplify the warming of surface fjord water, can have important implications for the long-term stability of the northern section of the Greenland Ice Sheet. We know that regional warming triggered sustained mass loss of the northeast Greenland ice sheet[35], and it has been suggested that reductions in ice mélange can destabilize floating ice tongues in high-latitude Greenland fjords[36–40]. For instance, Howat et al.[36] argued that high NST's, anomalously low sea ice concentration, and reduced mélange formation in 2003 triggered multi-year retreats of several marine-terminating glaciers on the Greenland west coast.

As sea-ice damming is effective in areas dominated by thick MYI, this should raise concerns for the accelerated retreat of outlet glaciers along the northern Greenland coast where the perennial sea ice cover is ever-present and thick (Fig. 1 and Supplementary Fig. S1). Higgins[41] concluded that sea ice was ever-present inside SOF between the years 1961 and 1985, but this seems to be becoming a less common feature in recent decades. Visual inspection of MODIS satellite images indicates that SOF was more or less clear from sea ice in 9 out the last 20 summers, with 2019 having the longest period of ice-free conditions (Supplementary Fig. S11). Although further analysis is needed in order to draw any definite conclusions, this indicates that a regime shift took place during the 1990s. In this context, it seems plausible that recent ice tongue breakups and retreats along the Greenland north coast, in Steensby, Ostenfeld, and Hagen Brae outlet glaciers[7] might have been associated with sea-ice damming, elevated NST's and subsequent loss of ice mélange in the corresponding fjords.

Conclusions

Although the summer of 2019 can currently be viewed as an outlier in terms of both average T_{2m} (4 °C warmer than present-day average) and SIC (almost three standard deviations below present-day average), both T_{2m} and SIC records show steep trends over the past decades, suggesting that today's extremes can soon become the new normal. In situ observations acquired from SOF show that these extreme atmospheric conditions had a strong impact on ocean temperature and chemistry. Observed NST's reached nearly 4 °C, which is about 3 °C higher than previously recorded in any ocean waters off northern Greenland. As a result of low near-surface salinities, the near-surface water of SOF was highly calcium carbonate-corrosive and twice as sensitive to ocean acidification by uptake of atmospheric CO_2 compared to outside the fjord and the nearby Petermann Fjord.

In this paper, we show that the remarkable marine response in SOF to the atmospheric forcing was related to damming of the surface water by thick pack ice at the mouth of the fjord. This notion is supported by the fact that the neighboring Petermann Fjord (with no sea ice outside) was not impacted in terms of temperature, salinity, or chemistry. This suggests that the year-round MYI off Greenland's north coast (Fig. 1), dramatically increases the sensitivity of adjacent fjords to climate change. As no NST time series is available in SOF, we do not know if similar warming has occurred before, but it seems likely that it will occur more frequently in the future. A linear extrapolation of T_{2m} and SIC suggests that the 2019 conditions would be the new normal by 2060, although feedback processes and emission scenarios could significantly alter such simple projection. Nevertheless, observed trends in T_{2m} and SIC over northern Greenland can have larger than expected destabilizing effects on marine-terminating Greenland glaciers draining into the Arctic Oceans, due to sea-ice damming and the associated increased climate sensitivity of fjords along the north Greenland coast.

Methods

CTD. Observations of temperature and salinity were made during the Ryder 2019 Expedition using a Seabird 911 CTD (conductivity, temperature, depth). The CTD was equipped with a 24 Niskin bottle (12 liters) rosette and the following sensors: Dual SeaBird temperature (SBE 3) and conductivity (SBE 04C), dissolved oxygen

(SBE 43), turbidity, and fluorescence (WET Labs ECO-AFL/FL) and a Benthos Altimeter PSA-916D. In situ conductivity and temperature have been converted to conservative temperature and absolute salinity using the TEOS-10 equation of state.

Satellite and reanalysis data. Sea ice thickness data in Fig. 1 are from CryoSat-2 Level-4 Sea-Ice Elevation, Freeboard, and Thickness, Version 1 data set (available from https://nsidc.org/data/RDEFT4/versions/1). The data set contains estimates of Arctic sea-ice thickness derived from the ESA CryoSat-2 Synthetic Aperture Interferometric Radar Altimeter (SIRAL). The data are provided on a 25 km grid as 30-day averages for the months between September and April[42].

CRUTEM4 is a global temperature dataset, providing gridded temperature land surface anomalies across the world, as well as averages for the hemispheres and the globe as a whole. Here we show data from CRUTEM.4.6.0.0 (available from https://www.metoffice.gov.uk/hadobs/crutem4/data/download.html).

Temperature data presented in Fig. 2a are from ERA5 reanalysis. The temperature represents that of air at 2 m above the surface of land, sea, or inland waters. It is calculated by interpolating between the lowest model level and the Earth's surface, taking account of the atmospheric conditions. Gridded monthly mean data (available from https://cds.climate.copernicus.eu/cdsapp#!/dataset/reanalysis-era5-single-levels-monthly-means) were averaged over June-August and over the area shown in Fig. 4f (dashed black) for each year.

The sea ice concentration presented in Fig. 2b is from Copernicus Climate Change Service. Data are derived from satellite passive microwave brightness temperatures from the series of SMMR, SSM/I, and SSMIS sensors. Sea ice concentration data were downloaded as daily gridded data from 1978 (available from https://cds.climate.copernicus.eu/cdsapp#!/dataset/satellite-sea-ice), and the average July-August values over three grid cells inside SOF (black crosses in Fig. 4f) were calculated for each year.

Chemistry–Data and analytical methods. Underway measurements of seawater pH[43] and TA[44] were taken every 10 min using spectrophotometric techniques (Contros HydroFIA pH and TA, Kiel, Germany) from the ship's underway system (bow intake at 8 m depth). Seawater pH was measured at S = 35 and 25° on the total scale. TA was measured at S = 35 and calibrated by routine calibrations of certified reference material (CRM Batch #181) obtained from A. G. Dickson of Scripps Institution of Oceanography (La Jolla, CA, USA). Both the seawater pH and TA data were post-processed and recalculated using the ship's underway salinity (SBE45) and temperature (SBE45) data. Discrete seawater pH was determined on the total scale employing a spectrophotometric method using the indicator m-Creosol Purple (mCP)[45,46]. The indicator was adjusted to a pH in the same range as the samples, approximately ±0.2 pH units, by adding a small volume of concentrated HCl or NaOH. Before running a set of samples, the pH of the indicator was measured using a 0.02 cm cuvette. The measurements were performed on board within hours of sampling and samples were thermostated to 25 °C in a water bath 30 min prior to analysis. An automatic system[47] was used where the sample and indicator were mixed in a syringe (Kloehn) before injected into a 1 cm cuvette of a diode array spectro-photometer (Agilent 8453), where the absorbance was measured at wavelengths 434, 578, and 730 nm, the latter accounting for background absorbance. The influence of indicator additions on the seawater pH samples was corrected for[47]. The pH values were corrected to 25 °C on the total scale. The accuracy was determined by the pureness of the indicator and by analyzing certified reference material (CRM batch #181). The latter measurements indicated that accuracy should be well below 0.01 pH unit. The precision as determined by replicates from the same sample bottle was in the range of ±0.001 pH unit. Discrete total alkalinity (TA) was determined using a semi-open cell potentiometric titration method using a 5-point Gran evaluation[48]. The system measures alkalinity in µmol/L using a nominal hydrochloric acid (HCl) concentration of 0.05 mol/L and 0.65 mol/L sodium chloride (NaCl). Certified reference material (CRM Batch #181) was used to determined accuracy. For all samples and CRM analyses, the alkalinity in µmol/kg was calculated using the salinity (from the CTD bottle file and the certified salinity, respectively) and the temperature measured at the beginning of the titration. Sample results were then multiplied with the factor determined from the CRM measurements at each individual station, and the correction was always below 0.5%. The given precisions were computed as standard deviations of duplicate analyses performed continually during the cruise. Duplicates were run from the same sample bottle since total alkalinity is not sensitive to atmospheric contamination with the results typically not deviating more than 2 µmol/kg.

Chemistry–Calculations of the carbonate system. All calculations concerning the marine carbonate system and buffer factors were done using *CO2SYS*.m ver 2.0[49,50] and *derivnum*.m[51], respectively. TA and seawater pH was used as the input parameters. The stoichiometric dissociation constants of carbonic acid of ref. [52] and the bisulfate constant of ref. [53] were used on the total scale at in situ temperatures as output conditions.

Data availability
Data presented in the paper are available from the Bolin Centre for Climate Research database; CTD sensor data[54] (https://bolin.su.se/data/ryder-2019-ctd), underway

measurements of seawater pH and total alkalinity[55] (https://bolin.su.se/data/ryder-2019-surface-seawater-ph-alkalinity) and seawater carbonate chemistry from CTD bottle samples[56] (https://bolin.su.se/data/ryder-2019-ctd-bottle-ph-alkalinity). Sea ice thickness data in Fig. 1 are from CryoSat-2 Level-4 Sea Ice Elevation, Freeboard, and Thickness, Version 1 data set, available from https://nsidc.org/data/RDEFT4/versions/1. CRUTEM.4.6.0.0 dataset is available from https://www.metoffice.gov.uk/hadobs/crutem4/data/download.html). ERA5 data are available from https://cds.climate.copernicus.eu/cdsapp#!/dataset/reanalysis-era5-single-levels-monthly-means Sea ice concentration data were downloaded as daily gridded data from 1978, available from https://cds.climate.copernicus.eu/cdsapp#!/dataset/satellite-sea-ice. MODIS-Terra corrected reflectance (true color) images obtained from the NASA Worldview webpage, worldview.earthdata.nasa.gov.

References
1. Kwok, R. Arctic sea ice thickness, volume, and multiyear ice coverage: losses and coupled variability (1958–2018). *Environ. Res. Lett.* **13**, 105005 (2018).
2. Maslanik, J., Stroeve, J., Fowler, C. & Emery, W. Distribution and trends in Arctic sea ice age through spring 2011. *Geophys. Res. Lett.* **38**, L13502 (2011).
3. Rothrock, D. A., Percival, D. B. & Wensnahan, M. The decline in arctic sea-ice thickness: Separating the spatial, annual, and interannual variability in a quarter century of submarine data. *J. Geophys. Res.* **113**, C05003 (2008).
4. Haas, C., Hendricks, S., Eicken, H. & Herber, A. Synoptic airborne thickness surveys reveal state of Arctic sea ice cover. *Geophys. Res. Lett.* **37**, L09501 (2010).
5. Kwok, R. et al. Thinning and volume loss of the Arctic Ocean sea ice cover: 2003–2008. *J. Geophys. Res.* **114**, C07005 (2009).
6. Laxon, S. W. et al. CryoSat-2 estimates of Arctic sea ice thickness and volume. *Geophys. Res. Lett.* **40**, 732–737 (2013).
7. Hill, E. A., Carr, J. R., Stokes, C. R. & Gudmundsson, G. H. Dynamic changes in outlet glaciers in northern Greenland from 1948 to 2015. *Cryosphere* **12**, 3243–3263 (2018).
8. Locarnini, R. A. et al. World Ocean Atlas 2013. Vol. 1: temperature. *A. Mishonov, Technical Ed. NOAA Atlas NESDIS* **73**, 40 (2013).
9. Jakobsson, M., Mayer, L. A., Farell, J. & Scientific Party. SWEDARCTIC-Ryder 2019 Report, v. 1. *Swedish Polar Research Secretariat* 1–455 (2020).
10. Jakobsson, M. et al. Ryder Glacier in northwest Greenland is shielded from warm Atlantic water by a bathymetric sill. *Commun. Earth Environ.* **1**, 1–10 (2020). 45.
11. Hersbach, H. et al. The ERA5 global reanalysis. *Quart. J. Royal Meteorol. Soc.* **146**, 1999–2049 (2020).
12. Jones, P. D. et al. Hemispheric and large-scale land-surface air temperature variations: an extensive revision and an update to 2010. *J. Geophys. Res.* **117**, RG2002 (2012).
13. Huang, J., Ou, T., Chen, D., Luo, Y. & Zhao, Z. The Amplified Arctic warming in the recent decades may have been overestimated by CMIP5 Models. *Geophys. Res. Lett.* **46**, 13338–13345 (2019).
14. Manabe, S. & Wetherald, R. T. The effects of doubling the CO_2 concentration on the climate of a general circulation model. *J. Atmos. Sci.* **32**, 3–15 (1975).
15. Serreze, M. C. & Barry, R. G. Processes and impacts of Arctic amplification: a research synthesis. *Global Planet Change* **77**, 85–96 (2011).
16. Stuecker, M. F. et al. Polar amplification dominated by local forcing and feedbacks. *Nat. Clim. Change* **8**, 1076–1081 (2018).
17. Cowtan, K. & Way, R. G. Coverage bias in the HadCRUT4 temperature series and its impact on recent temperature trends. *Quart. J. Royal Meteorol. Soc.* **140**, 1935–1944 (2014).
18. Screen, J. A. & Simmonds, I. The central role of diminishing sea ice in recent Arctic temperature amplification. *Nature* **464**, 1334 (2010).
19. Serreze, M. C., Barrett, A. P., Stroeve, J. C., Kindig, D. N. & Holland, M. M. The emergence of surface-based Arctic amplification. *Cryosphere* **3**, 11–19 (2009).
20. Miller, G. H. et al. Arctic amplification: can the past constrain the future? *Quat. Sci. Rev.* **29**, 1779–1790 (2010).
21. Tedesco, M. & Fettweis, X. Unprecedented atmospheric conditions (1948–2019) drive the 2019 exceptional melting season over the Greenland ice sheet. *Cryosphere* **14**, 1209–1223 (2020).
22. Sasgen, I. et al. Return to rapid ice loss in Greenland and record loss in 2019 detected by the GRACE-FO satellites. *Commun. Earth Environ.* **1**, 8 (2020).
23. Pemberton, P. & Nilsson, J. The response of the central Arctic Ocean stratification to freshwater perturbations. *J. Geophys. Res.* **121**, 792–817, (2015).
24. Rudels, B. Constraints on exchanges in the Arctic Mediterranean—do they exist and can they be of use? *Tellus A* **62**, 109–122 (2010).
25. Moon, T. et al. Subsurface iceberg melt key to Greenland fjord freshwater budget. *Nat. Geosci.* **11**, 49–54 (2018).

26. Veillette, J., Mueller, D. R., Antoniades, D. & Vincent, W. F. Arctic epishelf lakes as sentinel ecosystems: Past, present and future. *J. Geophys. Res.* **113**, G04014 (2008).

27. Bendtsen, J. et al. Sea ice breakup and marine melt of a retreating tidewater outlet glacier in northeast Greenland (81°N). *Scie. Rep.* **7**, 4941 (2017).

28. Hopwood, M. J. et al. Review article: How does glacier discharge affect marine biogeochemistry and primary production in the Arctic? *Cryosphere* **14**, 1347–1383 (2020).

29. Yamamoto-Kawai, M., McLaughlin, F. A., Carmack, E. C., Nishino, S. & Shimada, K. Aragonite Undersaturation in the Arctic Ocean: Effects of Ocean Acidification and Sea Ice Melt. *Science* **326**, 1098–1100 (2009).

30. Evans, W., Mathis, J. T. & Cross, J. N. Calcium carbonate corrosivity in an Alaskan inland sea. *Biogeosciences* **11**, 365–379 (2014).

31. Comeau, S., Gorsky, G., Alliouane, S. & Gattuso, J.-P. Larvae of the pteropod Cavolinia inflexa exposed to aragonite undersaturation are viable but shell-less. *Mar. Biol.* **157**, 2341–2345 (2010).

32. Fransson, A. et al. Late winter-to-summer change in ocean acidification state in Kongsfjorden, with implications for calcifying organisms. *Polar Biol.* **39**, 1841–1857 (2016).

33. Peck, V. L., Oakes, R. L., Harper, E. M., Manno, C. & Tarling, G. A. Pteropods counter mechanical damage and dissolution through extensive shell repair. *Nat. Commun.* **9**, 264 (2018).

34. Fabry, V. J., Seibel, B. A., Feely, R. A. & Orr, J. C. Impacts of ocean acidification on marine fauna and ecosystem processes. *ICES J. Mar. Sci.* **65**, 414–432 (2008).

35. Khan, S. A. et al. Greenland ice sheet mass balance: a review. *Rep. Prog. Phys.* **78**, 046801 (2015).

36. Howat, I. M., Box, J. E., Ahn, Y., Herrington, A. & McFadden, E. M. Seasonal variability in the dynamics of marine-terminating outlet glaciers in Greenland. *J. Glaciol.* **56**, 601–613 (2010).

37. Reeh, N., Thomsen, H. H., Higgins, A. K. & Weidick, A. Sea ice and the stability of north and northeast Greenland floating glaciers. *Ann. Glaciol.* **33**, 474–480 (2001).

38. Sohn, H.-G., Jezek, K. C. & Veen, C. J. van der. Jakobshavn Glacier, West Greenland: 30 years of spaceborne observations. *Geophys. Res. Lett.* **25**, 2699–2702 (1998).

39. Joughin, I. et al. Continued evolution of Jakobshavn Isbrae following its rapid speedup. *J. Geophys. Res.* **113**, F04006 (2008).

40. Joughin, I., Shean, D. E., Smith, B. E. & Floricioiu, D. A decade of variability on Jakobshavn Isbræ: ocean temperatures pace speed through influence on mélange rigidity. *Cryosphere* **14**, 211–227 (2020).

41. Higgins, A. K. North Greenland ice islands. *Polar Record* **25**, 207–212 (1989).

42. Kurtz, N. & Harbeck, J. CryoSat-2 Level 4 Sea Ice Elevation, Freeboard, and Thickness, Version 1, Boulder, Colorado USA. *NASA National Snow and Ice Data Center Distributed Active Archive Center* (2017).

43. Aßmann, S., Frank, C. & Körtzinger, A. Spectrophotometric high-precision seawater pH determination for use in underway measuring systems. *Ocean Sci.* **7**, 597–607 (2011).

44. Yao, W. & Byrne, R. H. Simplified seawater alkalinity analysis: Use of linear array spectrometers. *Deep Sea Res. Part I* **45**, 1383–1392 (1998).

45. Carter, B. R., Radich, J. A., Doyle, H. L. & Dickson, A. G. An automated system for spectrophotometric seawater pH measurements. *Limnol. Oceanogr.* **11**, 16–27 (2013).

46. Clayton, T. D. & Byrne, R. H. Calibration of m-cresol purple on the total hydrogen ion concentration scale and its application to CO_2-system characteristics in seawater. *Deep-Sea Res.* **40**, 5–2129 (1993).

47. Fransson, A., Engelbrektsson, J. & Chierici, M. Development and optimization of a Labview program for spectrophotometric pH measurements of seawater, pHspec ver 2.5. University of Gothenburg (2013).

48. Haraldsson, C., Anderson, L. G., Hassellöv, M., Hulth, S. & Olsson, K. Rapid, high-precision potentiometric titration of alkalinity in ocean and sediment pore waters. *Deep Sea Res. Part I* **44**, 2031–2044 (1997).

49. Lewis, E., Wallace, D. & Allison, L. J. *Program developed for CO {sub 2} system calculations*. United States: N. p., Web. https://doi.org/10.2172/639712 (1998).

50. Van Heuven, S., Pierrot, D., Rae, J. W. B., Lewis, E. & Wallace, D. W. R. MATLAB program developed for CO_2 system calculations. *ORNL/CDIAC-105b. Carbon Dioxide Information Analysis Center, Oak Ridge National Laboratory, US Department of Energy, Oak Ridge, Tennessee.* 530 (2011).

51. Orr, J. C., Epitalon, J.-M., Dickson, A. G. & Gattuso, J.-P. Routine uncertainty propagation for the marine carbon dioxide system. *Marine Chem.* **207**, 84–107 (2018).

52. Lueker, T. J., Dickson, A. G. & Keeling, C. D. Ocean pCO2 calculated from dissolved inorganic carbon, alkalinity, and equations for K1 and K2: validation based on laboratory measurements of CO_2 in gas and seawater at equilibrium. *Marine Chem.* **70**, 105–119 (2000).

53. Dickson, A. G. Standard potential of the reaction: AgCl(s) + 12H2(g) = Ag(s) + HCl(aq), and and the standard acidity constant of the ion HSO4− in synthetic sea water from 273.15 to 318.15 K. *J. Chem. Thermodyn.* **22**, 113–127 (1990).

54. Stranne, C., Nilsson, J., Muchowski, J. & Chawarski, J. Oceanographic CTD data from the Ryder 2019 expedition. *Bolin Centre Database* Dataset version 1.0 https://doi.org/10.17043/ryder-2019-ctd. (2020).

55. Ulfsbo, A. Underway measurements of seawater pH and total alkalinity from the Ryder 2019 expedition. *Bolin Centre Database* Dataset version 1.0. https://doi.org/10.17043/ryder-2019-surface-seawater-ph-alkalinity. (2021).

56. Ulfsbo, A., Stranne, C. & Nilsson, J. Seawater carbonate chemistry from CTD bottle samples during the Ryder 2019 expedition. *Bolin Centre Database* Dataset version 1.0. https://doi.org/10.17043/ryder-2019-ctd-bottle-ph-alkalinity. (2021).

Author contributions

C.S. and J.N. conceived the original idea of the paper. All other authors (M.J., A.U., M.O., H.K.C., L.M., J.M., L.A.M., V.B., J.F., B.T., J.C., G.W., and E.W.) have provided input on the paper and participated in various ways in the data collection and processing.

Competing interests

The authors declare no competing interests.

Additional information

Supplementary information The online version contains supplementary material available at https://doi.org/10.1038/s43247-021-00140-8.

Correspondence and requests for materials should be addressed to C.S.

Peer review information Primary handling editor: Heike Langenberg.

Reprints and permission information is available at http://www.nature.com/reprints

Publisher's note Springer Nature remains neutral with regard to jurisdictional claims in published maps and institutional affiliations.